Data supplement for Xu et al., Antibodies From Children With PANDAS Bind Specifically to Striatal Cholinergic Interneurons and Alter Their Activity. Am J Psychiatry (doi: 10.1176/appi.ajp.2020.19070698)

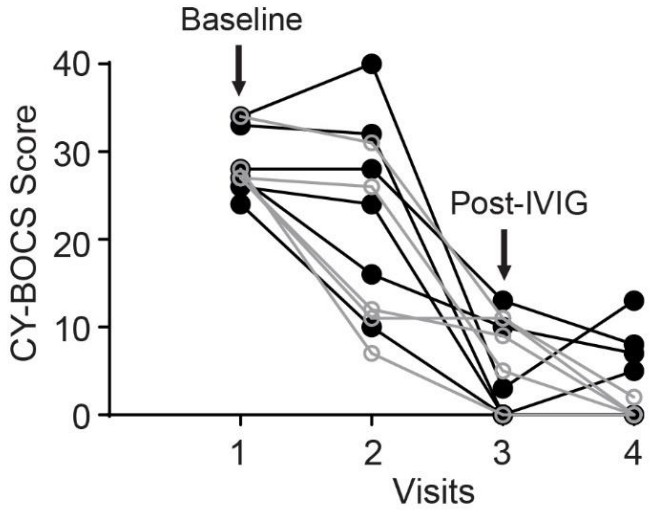

FIGURE S1. Response to intravenous immunoglobulin (IVIG) treatment in subjects used in the study (cohorts #1 and #2). The Children's Yale-Brown Obsessive Compulsive Scale (CY-BOCS) score was evaluated in at baseline (visit 1) and at 6 weeks (visit 2), 3 months (visit 3) and 6 months (visit 4) in children diagnosed with PANDAS (1). Sera from baseline (visit 1) and 3 month (visit 3) were used for the serum assays described in the main text. Subjects received either IVIG or placebo, double-blind, at time point 1 (after ratings were collected), and then had the option to receive IVIG open-label at time point 2 (after ratings); thus at time point 3 all subjects had received one or two doses of IVIG, 6-12 weeks previously. These subjects were specifically selected on the basis of their positive IVIG response during either the blinded or the open-label phase of the trial. Open circles indicate the 5 subjects whose sera were characterized in a previous study (2) (Cohort #1). Closed circles indicate 6 additional subjects whose sera are characterized for the first time in the current study (Cohort #2). Subject demographics are given in Table S1.

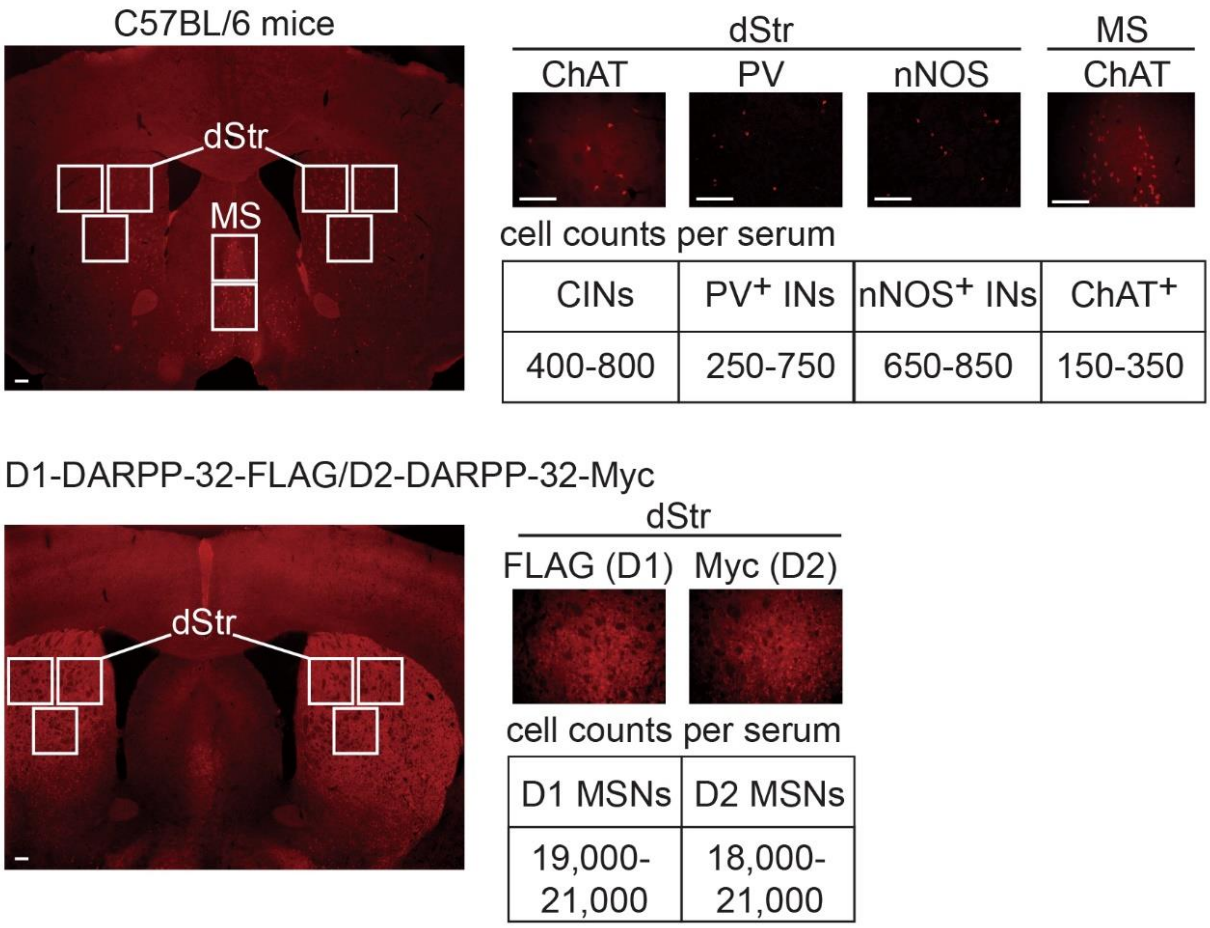

FIGURE S2. Schematic diagram of unbiased imaging process. Male and female C57BL/6 and D1-DARPP-32-FLAG/D2-DARPP-32-Myc (3, 4) mouse brain sections were used for immunohistochemical staining. Six images per slice were obtained in dorsal striatum (dStr) for cholinergic interneurons (CINs), parvalbumin-positive interneurons (PV^+ INs), neuronal nitric oxide synthase-positive interneurons ($nNOS^+$ INs), D1 medium spiny neurons (D1 MSNs) and D2 MSNs. Two images per slice were obtained in medial septum (MS) for cholinergic neurons ($ChAT^+$). Total cells scored for each neuronal type are as indicated. Scale bar: 100 μm.

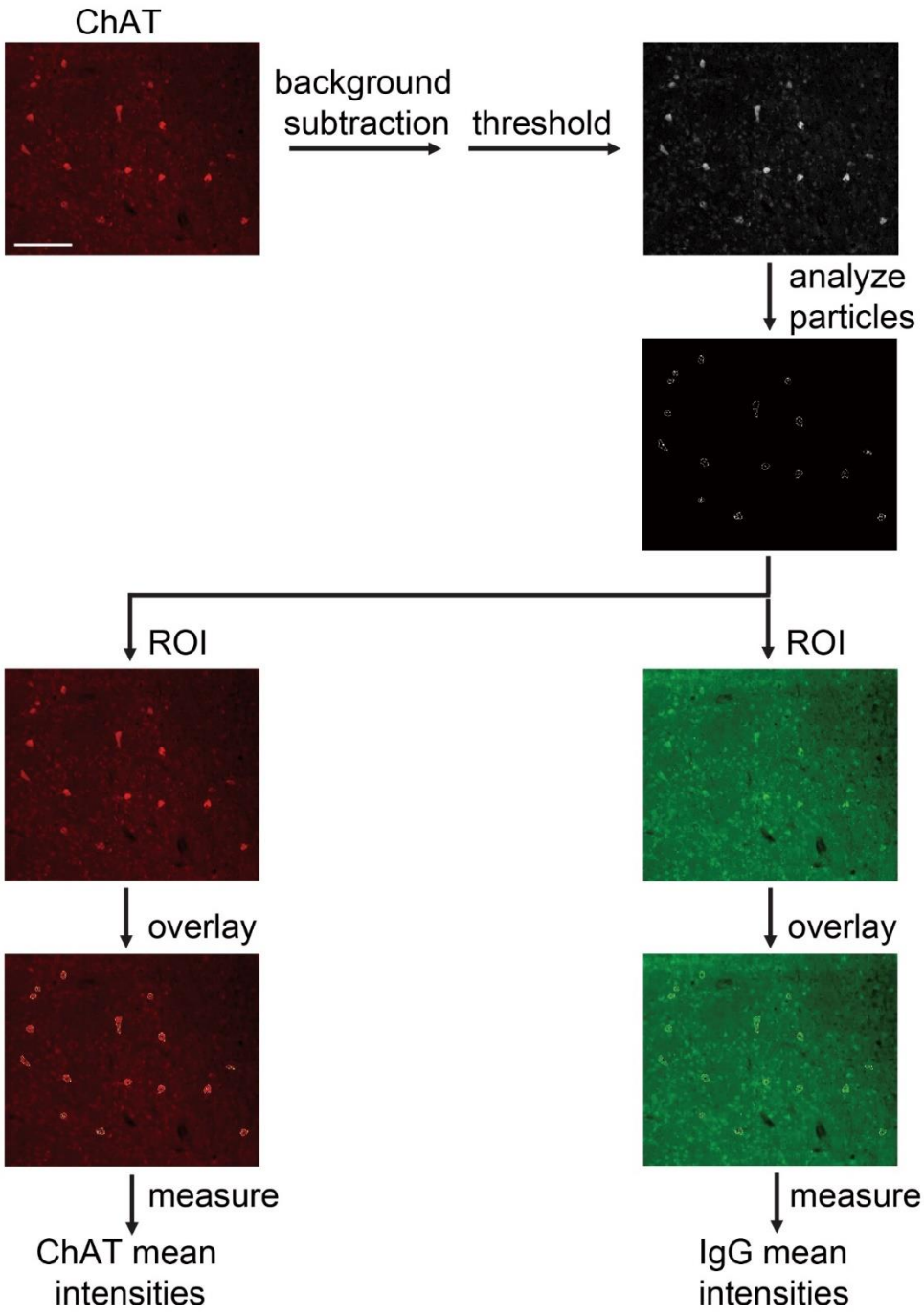

FIGURE S3. Automated quantitation of IgG deposition to different neuronal types using Fiji program. IgG binding to striatal cholinergic interneurons is shown as an example. Striatal slices were immunostained with anti-ChAT and anti-human IgG antibodies and visualized using fluorophore-conjugated secondary antibodies. Images were taken using a fluorescent microscope under the same settings for all the sera. A ChAT image was used to generate a filter with cell outlines as regions of interest. The filter was then overlayed with the corresponding anti-human IgG image to mark the area for quantitation. Mean fluorescence intensity (pixels) was measured. All the images were processed using the batch processing function in Fiji. Additional background subtraction was applied to get the adjusted values of each cell. Scale bar: 100 μm.

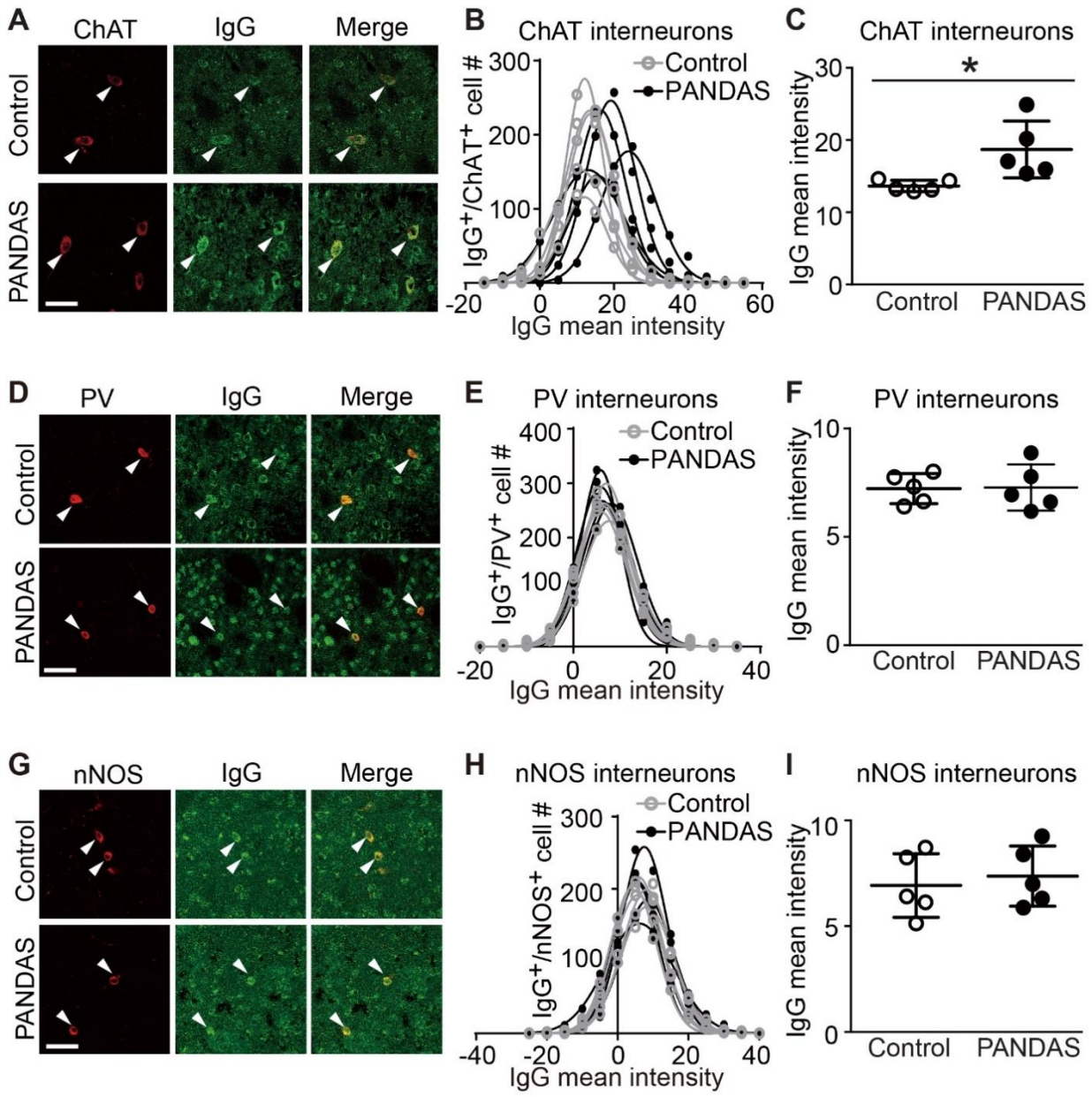

FIGURE S4. Replication of elevated PANDAS IgG binding to striatal cholinergic interneurons in the original 5 samples. (A) Illustrative confocal images of immunohistochemical staining of human IgG (green) and choline acetyltransferase (ChAT, red). 'Merge' images combine both channels to illustrate overlap. Arrowheads indicate human IgG binding to ChAT-positive neurons (cholinergic interneurons, CINs). Scale bar: 40 μm. (B) Gaussian distribution of mean IgG immunofluorescence within striatal CINs, identified by ChAT immunoreactivity, for PANDAS and control sera. (C) IgG binding to CINs was higher after incubation with PANDAS sera than after incubation with control sera (independent sample t-test: $t[8]=2.810$, $p=0.023$). (D) Confocal images of immunohistochemical staining of anti-human IgG (green) and anti-parvalbumin (PV, red). Arrowheads indicate antibody binding to PV-positive interneurons. (E) Gaussian distribution of the mean fluorescence intensity of IgG^+/PV^+ double-positive neurons for PANDAS and control sera. (F) IgG binding to PV-positive interneurons

does not change in both groups ($t[8]=0.096$, $p>0.9$). (G) Confocal images of immunostaining of anti-human IgG (green) and anti-neuronal nitric oxide synthase (nNOS, red). Arrowheads indicate antibody binding to nNOS-positive interneurons. (H) Gaussian distribution of the mean fluorescence intensity of $IgG^+/nNOS^+$ double-positive neurons for PANDAS and control sera. (I)There is no group difference in IgG binding to nNOS-positive interneurons ($t[8]=0.476$, $p>0.6$). . Scale bar: 40 μm. *$p<0.05$, N=5 each group. Representative images of single-photon immunofluorescence used in quantification are shown in Figure S16A-S16C.

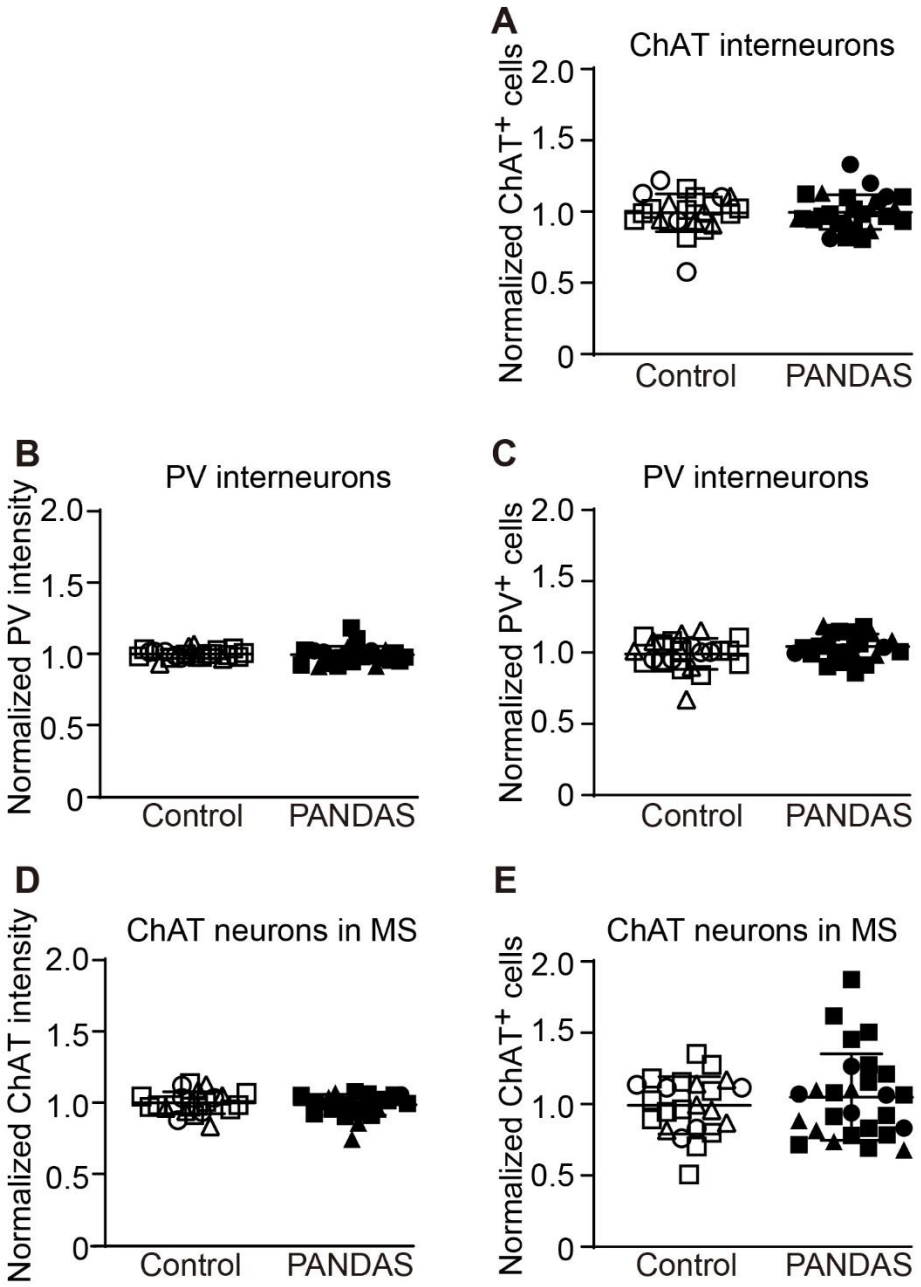

FIGURE S5. No difference in the fluorescence intensity of PV or ChAT, or the total cells scored between groups. Data are shown for all 50 samples across 3 patient and control cohorts. (A) Total $ChAT^+$ interneurons counted do not differ between control and PANDAS groups (independent sample t-test: $t[48]=0.139$, $p>0.8$). (B) PV staining remains unchanged between the groups ($t[48]=0.481$, $p>0.6$). (C) Total PV^+ interneurons counted do not differ between the groups ($t[48]=1.793$, $p=0.079$). (D) Mean fluorescence intensity of ChAT does not change in the medial septum (MS, $t[48]=0.648$, $p>0.5$). (E) Total $ChAT^+$ neurons in the MS do not differ between the groups ($t[48]=0.780$, $p>0.4$). N=27 for PANDAS group and N=23 for control group. ●,○ – 10 serum from the first cohort (2); ▲,△ – 12 sera in the second cohort; ■,□ – 28 sera in the third cohort.

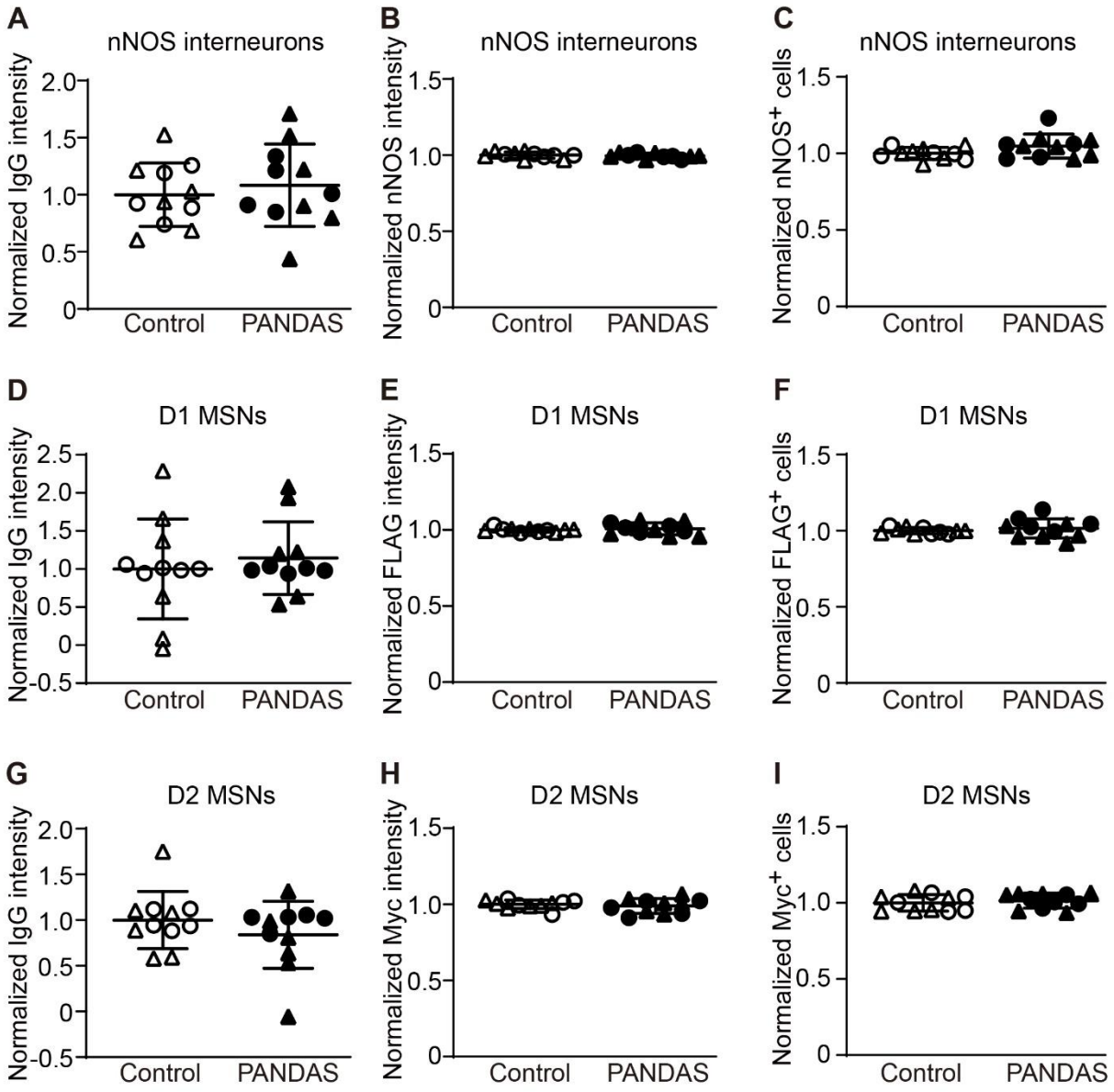

FIGURE S6. PANDAS antibodies show similar binding to nNOS interneurons and to D1 and D2 medium spiny neurons in the first and second cohorts of 11 samples. (A) PANDAS antibodies bind to nNOS interneurons at comparable levels to controls ($t[20]=0.605$, $p>0.5$) (B) nNOS staining remains unchanged between the groups ($t[20]=0.535$, $p>0.5$). (C) Total $nNOS^+$ cells counted do not differ ($t[20]=1.803$, $p=0.086$). (D) There is no group difference between control and PANDAS in IgG binding to dopamine D1 receptor positive ($D1R^+$) medium spiny neurons ($t[20]=0.583$, $p>0.5$). (E) FLAG staining remains unchanged between the groups ($t[20]=0.572$, $p>0.5$). (F) Total $D1R^+$ cells do not differ between the groups ($t[20]=0.765$, $p>0.5$). (G) There is no difference in IgG binding to dopamine D2 receptor positive ($D2R^+$) medium spiny neurons between the groups ($t[20]=1.113$, $p=0.279$). (H) Myc staining remains unchanged between the groups ($t[20]=0.624$, $p>0.5$). (I) Total $D2R^+$ cells counted do not differ between the groups ($t[20]=0.676$, $p>0.5$). N=11 for control and PANDAS groups. ●,○ – 10 serum from the first cohort (2); ▲,△ – 12 sera in the second cohort.

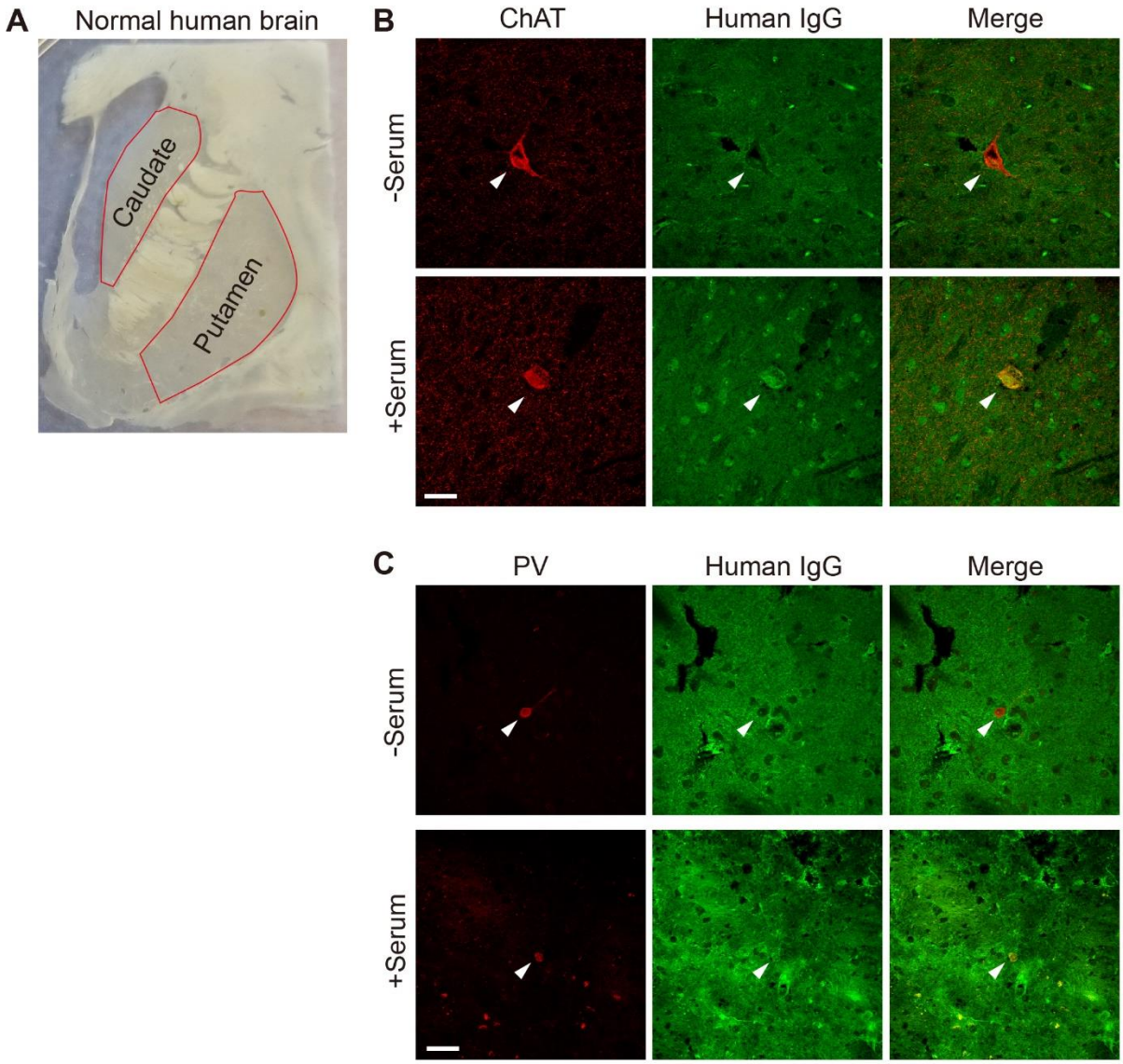

FIGURE S7. Pilot study on serum IgG binding to normal human brain. (A) Caudate and putamen (outlined) were excised from human brain sections, incubated with or without a control serum (1.25 mg/dL, overnight at 4 °C), followed by triple-labeling using anti-human IgG, anti-ChAT and anti-PV antibodies. (B) Representative confocal image of immunohistochemical staining of human IgG (green) and ChAT (red) in human caudate. 'Merge' images combine both channels to illustrate overlap. Arrowheads indicate human IgG binding to cholinergic interneurons. (C) Representative confocal image of immunohistochemical staining of human IgG (green) and PV (red) in human caudate. Arrowheads indicate human IgG binding to PV interneurons. Scale bar: 40 μm. There was no IgG staining in CINs or PV-interneurons in the absence of serum incubation.

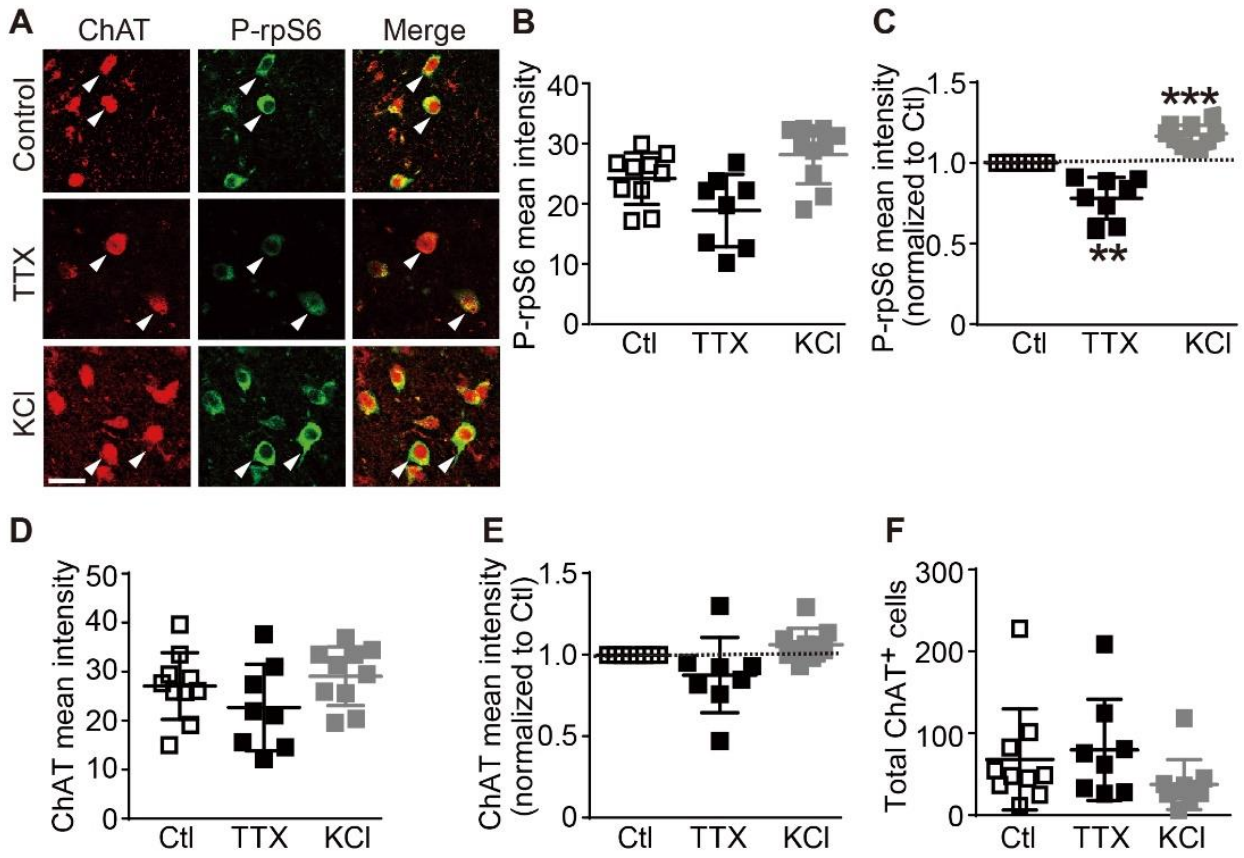

FIGURE S8. Tetrodotoxin and KCl induce changes in the phosphorylation of rpS6 in striatal CINs. Acute striatal slices were treated with control (aCSF with 0.1% DMSO), tetrodotoxin (TTX, 1 μM, 0.1% DMSO final concentration) or KCl (20 mM) for 1 h. (A) Confocal images of co-staining of anti-phospho-rpS6 (green) and anti-ChAT (red) in striatal slices after treatment. 'Merge' images combine both channels to illustrate overlap. Arrowheads indicate expression of P-rpS6 in striatal ChAT interneurons. Scale bar: 40 μm. Representative images of immunostaining used in quantification are shown in Figure S18A. (B) Mean fluorescence intensity of P-rpS6 staining in 10 independent replicates (one-way ANOVA: $F[2,25]=7.594$, $p=0.003$; TTX vs control: $p=0.085$, Tukey's multiple comparison test). (C) Normalizing to saline-treated slices in each experiment reduces variance and clarifies these effects (TTX: two-tailed one-sample t-test, $t[7]=4.768$, $p=0.002$; KCl: $t[9]=7.655$, $p<0.0001$); these effects are consistent with previous findings (5). (D, E) Mean ChAT immunofluorescence in stained CINs; data in (E) are normalized to control. (F) Total number of ChAT-positive neurons counted in each group do not differ. **$p<0.01$, ***$p<0.001$, N=10 for control and KCl, N=8 for TTX.

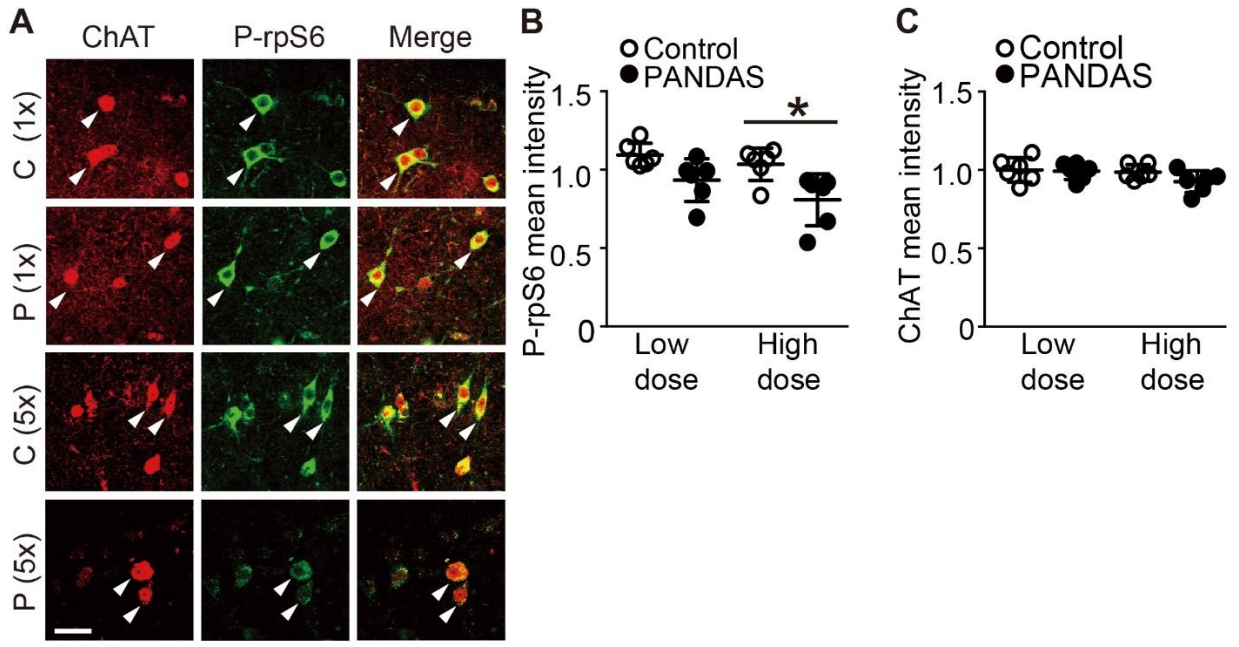

FIGURE S9. Pilot experiment to determine serum titer for characterization of regulation of CIN activity in acute brain slices. Serum from 1 PANDAS subject and matched control were selected based on the greatest difference in binding to CINs (Figure 1C). Sera were incubated with striatal slices in aCSF at low dose (1×, the same IgG titer used in *ex vivo* staining, 1.25 mg/dL) or high dose (5×, 6.25 mg/dL) for 1 h. After this treatment, slices were briefly fixed, and then immunostained for ChAT and phospho-rpS6 (P-rpS6). (A) Confocal images of co-immunostaining for P-rpS6 (green) and ChAT (red). 'Merge' images combine both channels to illustrate overlap. Arrowheads indicate expression of P-rpS6 in CINs. Scale bar: 40 μm. (B) Mean P-rpS6 immunofluorescence, normalized to saline-treated slices run in parallel for each of six independent replication experiments, was reduced after treatment with PANDAS serum, compared with control serum (2-way ANOVA: $F[1,20]=14.400$, $p=0.001$; high dose, PANDAS vs control, $p=0.024$, Tukey's multiple comparison test). (C) ChAT immunofluorescence, normalized to saline-treated control, showed no difference between the control and PANDAS group. *$p<0.05$. N=6 for each group).

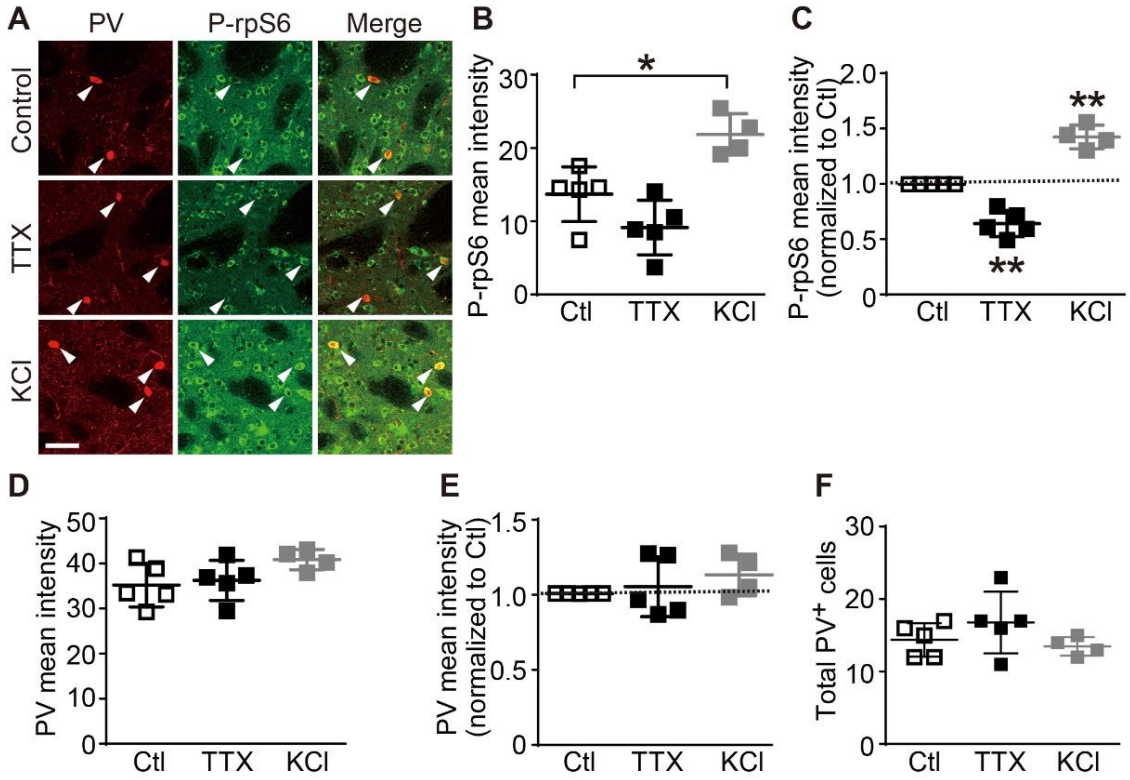

FIGURE S10. Tetrodotoxin and KCl alters phosphorylation levels of rpS6 in striatal PV-interneurons. Acute striatal slices were treated with control (aCSF with 0.1% DMSO), tetrodotoxin (TTX, 1 μM, 0.1% DMSO final concentration) or KCl (20 mM) for 1 h. (A) Confocal images of co-staining of P-rpS6 (green) and PV (red) in striatal slices after treatment. 'Merge' images combine both channels to illustrate overlap. Arrowheads indicate expression of P-rpS6 in striatal PV-interneurons. Scale bar: 40 μm. Representative images of immunostaining used in quantification are shown in Figure S18C. (B) Mean fluorescence intensity of P-rpS6 staining in 5 independent replicates (one-way ANOVA: $F[2,11]=14.740$, $p=0.0008$; KCl vs control: $p=0.0134$, Tukey's multiple comparison test). (C) Normalizing to control-treated slices in each experiment reduces variance and clarifies these effects (TTX: two-tailed one-sample t-test, $t[4]=6.713$, $p=0.0026$; KCl: two-tailed one-sample t-test, $t[3]=8.087$, $p<0.004$). (D, E) Mean PV immunofluorescence in stained CINs; data in (E) are normalized to control. (F) Total number of PV-positive neurons counted in each group do not differ. *$p<0.05$, **$p<0.01$, N=5 for control and TTX, N=4 for KCl.

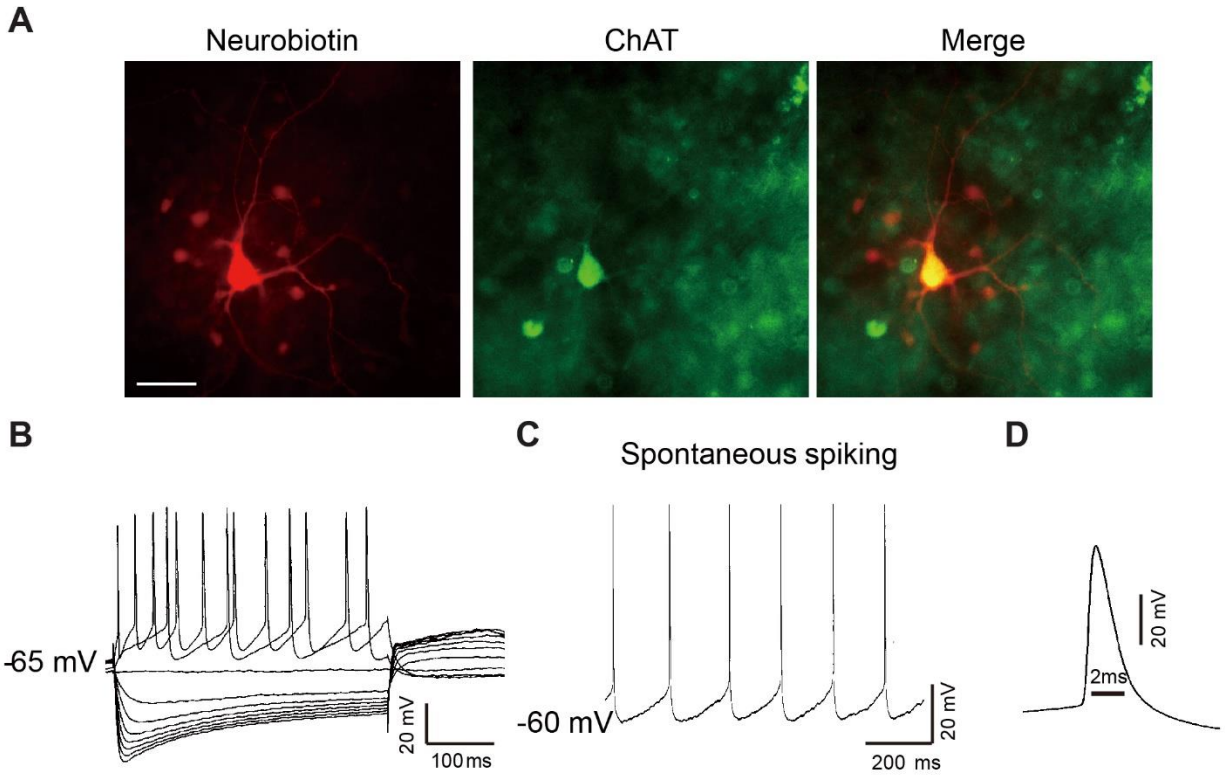

FIGURE S11. Morphological and electrophysiological features of striatal cholinergic interneurons. (A) Micrograph of a large CIN filled with neurobiotin in a striatal slice and subsequently labelled with streptavidin (red) and ChAT (green) to identify recorded cholinergic interneurons. 'Merge' images combine both channels to illustrate overlap. Scale bar: 40 μm. (B) In a representative recording, depolarizing somatic current injection (500 pA, 400ms) induced a train of action potentials showing a large AHP; hyperpolarizing current injection (500pA, 400ms) induced a typical sag in the membrane response, indicating strong Ih. (C, D) Representative trace showing spontaneous spike (C) and wide action potential with an amplitude almost exceeding 2 ms (D).

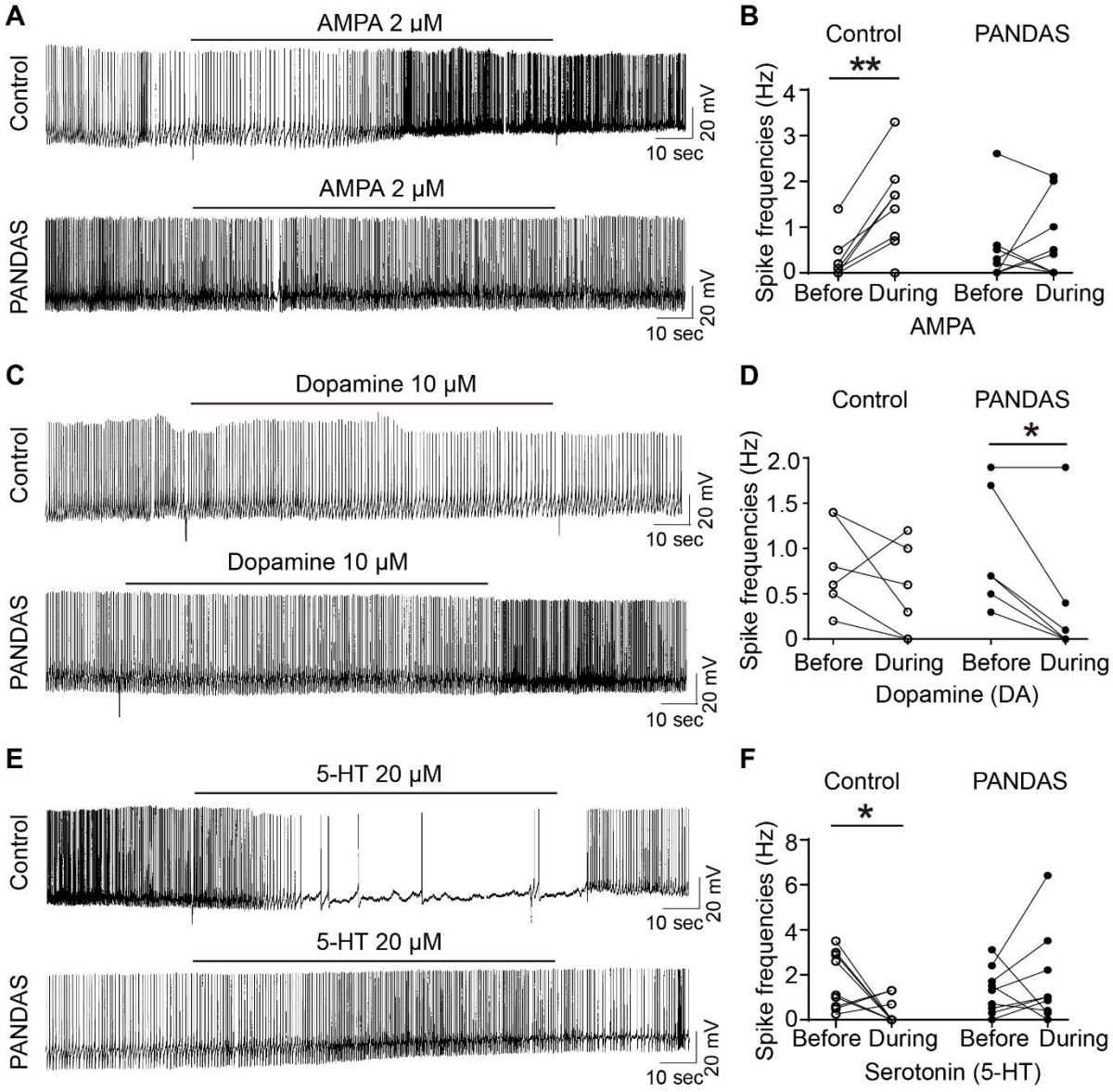

FIGURE S12. PANDAS serum alters neurotransmitter response in striatal CINs. Acute striatal slices were pretreated with control or PANDAS serum (6.25 mg/dL for 1 h); CINs were then recorded using whole-cell patch clamp. A single serum pair was tested in multiple independent recordings. Basal electrophysiological properties of CINs are shown in Figure S11. Slices were treated with AMPA (A and B), DA (C and D) or 5-HT (E and F) at the indicated doses. The scale bars are 10 s and 20 mV. (A, C and E) Representative traces of spontaneous spikes from neurotransmitter-treated CINs in control- and PANDAS serum pretreated striatal slices. (B) AMPA increases firing in CINs pre-treated with control serum, but not in CINs pretreated with PANDAS serum (2-way RM-ANOVA: main effect of AMPA, $F[1,14]=12.45$, $p=0.0033$; main effect of serum not significant; interaction: $F[1,14]=5.7$, $p=0.03$; control: N=7 cells; PANDAS: N=6 cells). (D) DA treatment produced no consistent effect in CINs pre-treated with control serum but caused a significant decrease in firing in CINs pre-treated with PANDAS serum; the interaction was not significant in this case (2-way RM-ANOVA: main effect of DA, $F[1,10]=9.11$, $p=0.0129$; main effect of serum NS: interaction, $F[1,10]=0.863$,

p>0.35; N=6 cells for both control and PANDAS). (F) 5-HT had a complex effect on CIN firing in control serum-pretreated slices, increasing the firing of some cells but silencing others completely. The ability of 5-HT to silence CINs was lost in slices pre-treated with PANDAS serum (2-way RM-ANOVA; main effects of serum and 5-HT not significant; interaction: $F[1,16]=4.428$, $p=0.05$; control: N=9 cells; PANDAS: N=7 cells). Post-hoc two-tailed paired t-test: * $p<0.05$; ** $p<0.01$.

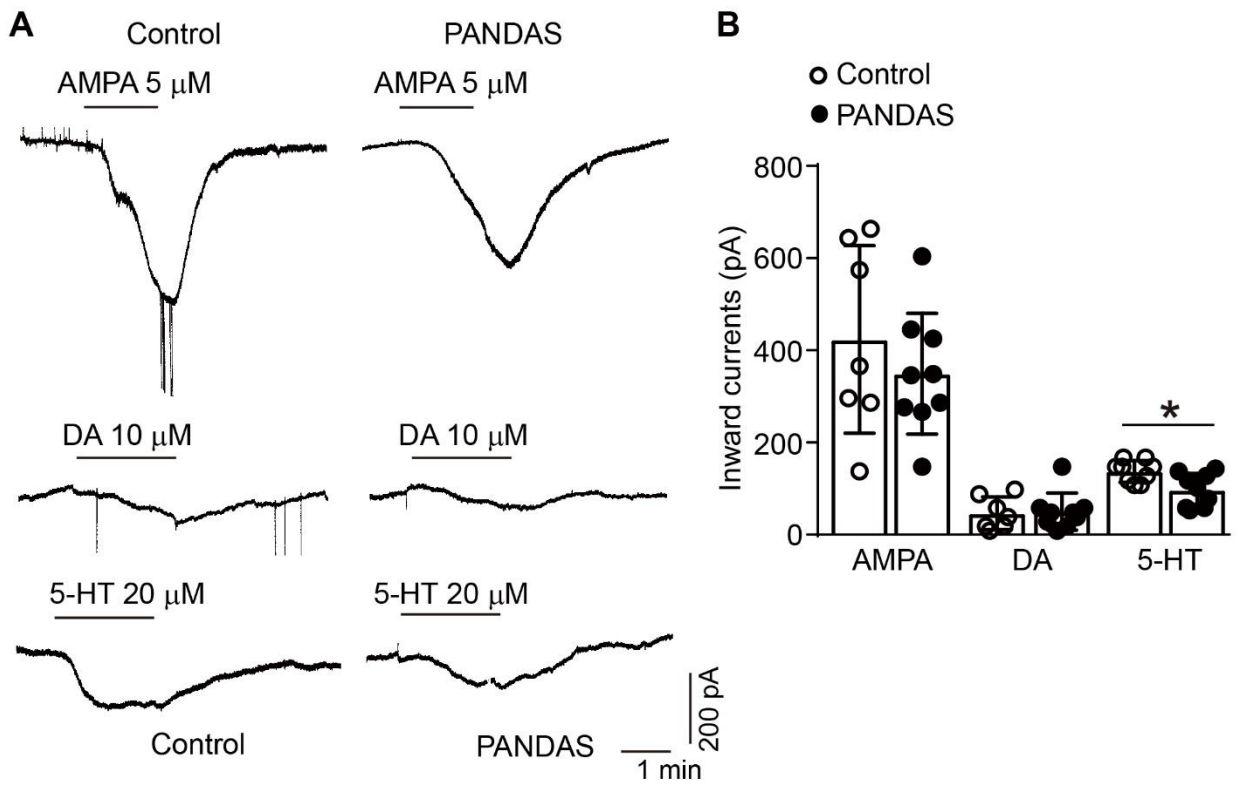

FIGURE S13. Inward currents after AMPA, DA, or 5-HT in CINs pretreated with control or PANDAS serum. Acute striatal slices were pretreated with control or PANDAS serum (6.25 mg/dL for 1 h); CINs were then recorded using whole-cell patch clamp. (A) Representative current traces induced in CINs by AMPA, Dopamine (DA), and serotonin (5-HT). (B) PANDAS serum does not alter AMPA-induced inward current ($t[14]=0.889$, $p>0.35$) or DA-induced inward current ($t[14]=0.188$, $p=0.854$), but induces a significant reduction in 5-HT-induced inward current (unpaired two-tailed t-test: $t[16]=2.805$, $p=0.013$), compared with control serum. Control: N=7 cells for AMPA, N=9 cells for DA, N=9 cells for 5-HT; PANDAS: N=9 cells for AMPA, N=9 cells for DA, N=9 cells for 5-HT. *$p<0.05$.

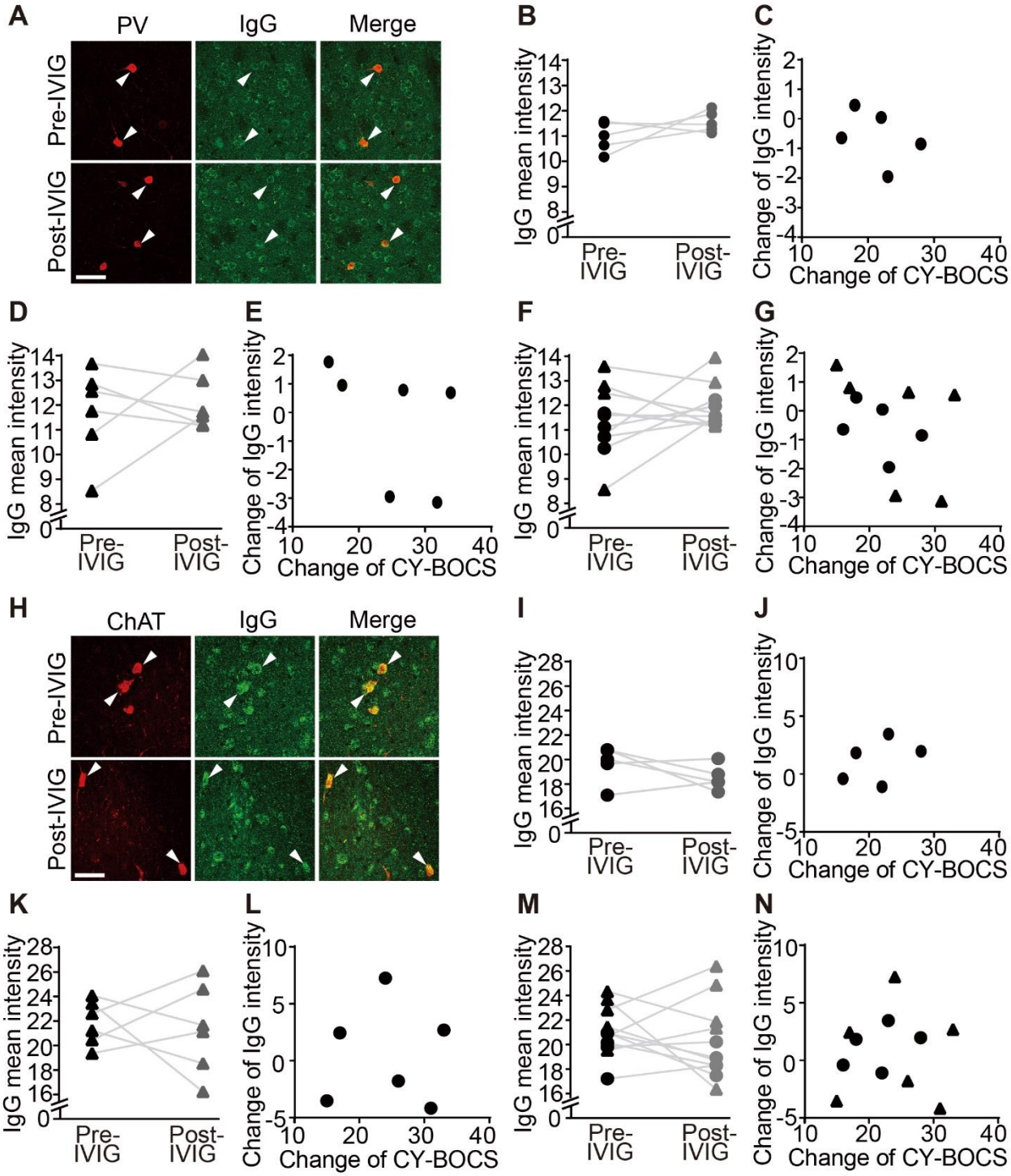

FIGURE S14. IVIG treatment does not alter PANDAS antibody binding to PV interneurons or to ChAT neurons in the medial septum. Serum samples from baseline (pre-IVIG) and 3 months after IVIG treatment (post-IVIG) were tested. (A) Confocal images of co-staining of anti-human IgG (green) and anti-PV (red) before and after IVIG treatment. 'Merge' images combine both channels to illustrate overlap. Arrowheads indicate antibody binding to PV positive interneurons. Scale bar: 40 μm. Representative images of immunostaining used in quantification are shown in Figure S17B. (B, D, F) IVIG treatment does not change PANDAS

IgG binding to PV interneurons in (B) the original 5 sera (paired t-test: t[4]=1.415, p=0.230), (D) the second cohort (paired t-test: t[5]=0.485, p=0.648), or (F) both cohorts combined (paired t-test: t[10]=1.031, p=0.327). (C, E, G) Changes in PANDAS IgG binding to PV interneurons following IVIG treatment show no relationship with the Children's Yale-Brown Obsessive Compulsive Scale (CY-BOCS) score in (C) the original 5 sera (paired t-test: t[4]=1.383, p=0.239), (E) the second cohort (paired t-test: t[5]=0.270, p=0.780), or (G) pooled data (paired t-test: [10]=0.781, p=0.453). (H) Confocal images of co-staining of anti-human IgG (green) and anti-ChAT (red) before and after IVIG treatment in the medial septum. Arrowheads indicate antibody binding to ChAT positive neurons. Representative images of immunostaining used in quantification are shown in Figure S17C. Scale bar: 40 μm. (I, K, M) IVIG treatment does not change PANDAS IgG binding to ChAT neurons in the medial septum in the original 5 sera (I), the second cohort (K) and both cohorts combined (M). (J, L, N) Changes in PANDAS IgG binding to ChAT neurons following IVIG treatment show no relationship with the CY-BOCS score in the original 5 sera (J), the second cohort (L) and both cohorts combined (N). ●,○ – 10 serum from the first cohort (2); ▲,△ – 12 sera in the second cohort.

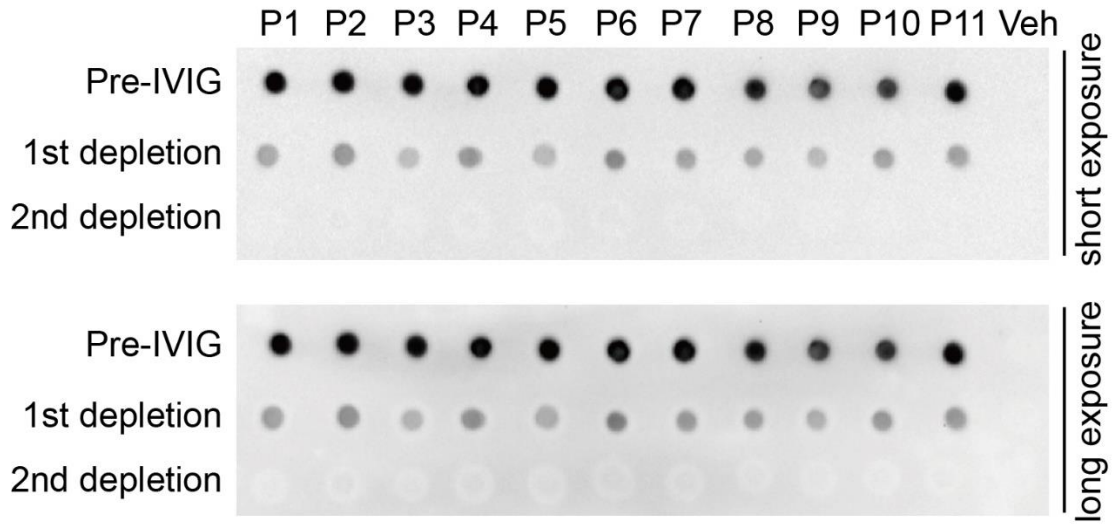

FIGURE S15. IgG depletion in pre-IVIG PANDAS sera. Pre-IVIG PANDAS sera of 11 subjects (Table S1) were incubated with Protein A/G agarose beads for 2 h at 4 °C. Supernatants were collected by brief centrifugation (1000×g for 1 min) and mixed with fresh Protein A/G agarose beads for a second round depletion. Small aliquots from both batches of supernatants were tested on dot blot using a rabbit anti-human IgG antibody and HRP-conjugated goat anti-rabbit secondary antibody (Table S3). Membranes were developed using a chemiluminescent substrate kit. IgG was completely depleted after two rounds of purification. Supernatants of the 2nd depletion were used in Figure 5 as S1-depleted.

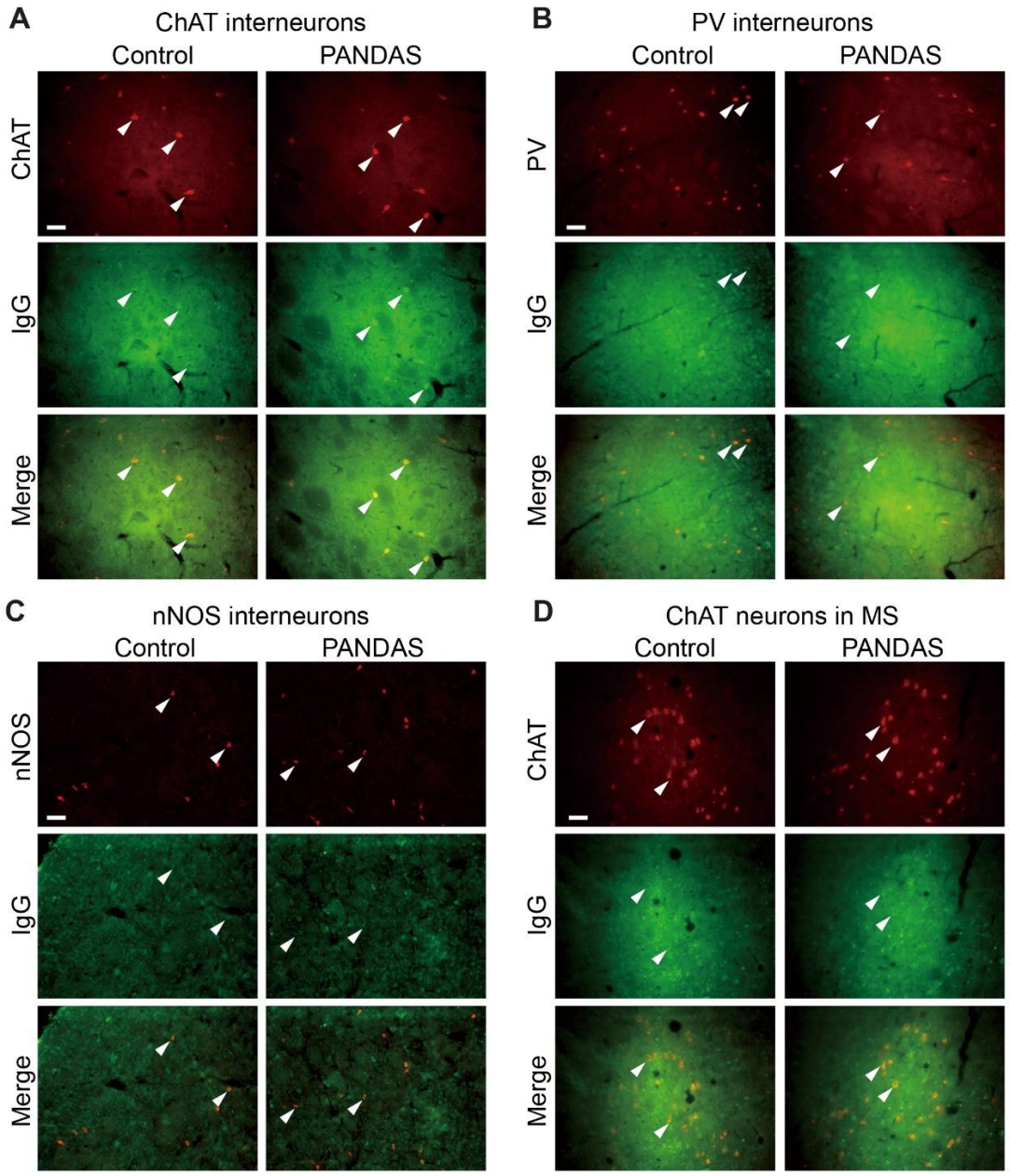

FIGURE S16. Representative images of serum IgG binding to several neuronal types. C57BL/6 mice striatal slices were co-labeled with human IgG (green) and different neuron markers ChAT (A), PV (B), nNOS (C) and ChAT in medial septum (D). Images were taken under 20× object using an epifluorescence microscope with consistent acquisition settings. 'Merge' images combine both channels to illustrate overlap. Scale bar: 40 μm. Uncropped images were used for automated quantification. Confocal images at higher magnification (40×) are shown in Figure 1A, S4A.

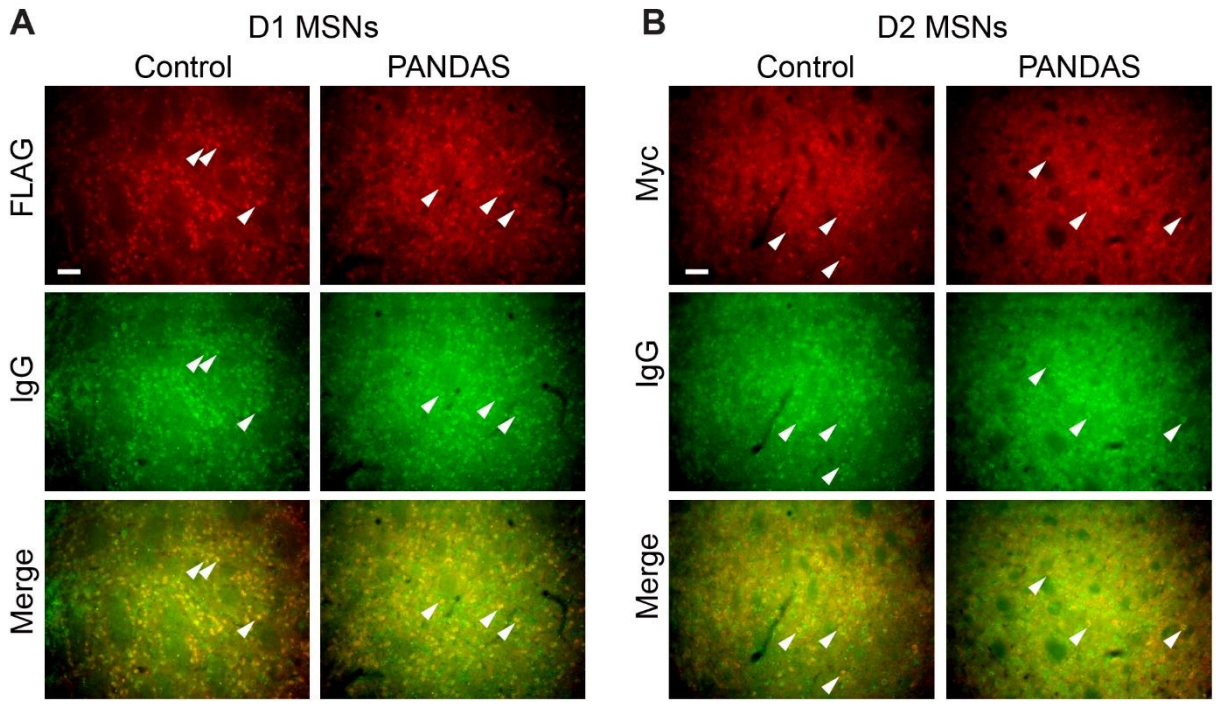

FIGURE S17. Representative images of serum IgG binding to D1 and D2 MSNs[a]. [a]D1-DARPP-32-FLAG/ D2-DARPP-32-Myc mice striatal slices were co-labeled with human IgG (green) and D1 MSNs marker FLAG (A) or D2 MSNs marker Myc (B). Images were taken under 20× object using an epifluorescence microscope with constant setting. 'Merge' images combine both channels to illustrate overlap. Scale bar: 40 μm. Uncropped images were used for automated quantification. Results of quantification are shown in Figure S6.

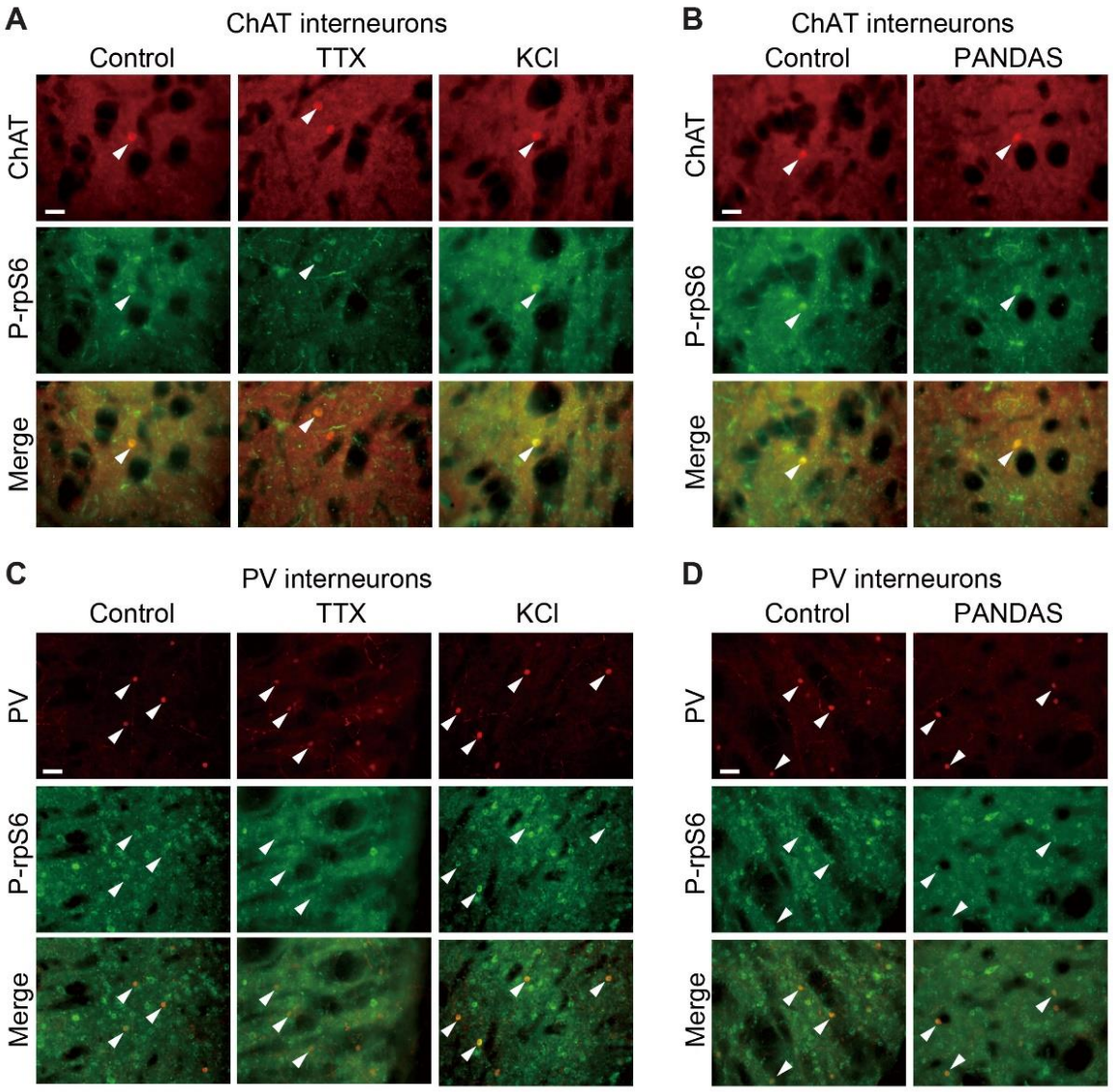

FIGURE S18. Representative images of P-rpS6 staining after serum and controls treatment in acute brain slices. (A, C) Acute striatal slices from C57BL/6 mice were incubated with control groups: control (aCSF+0.1% DMSO), TTX (1 μM, 0.1% DMSO final concentration) and KCl (20 mM). (B, D) Acute striatal slices were incubated with control and PANDAS serum. After treatment, slices were co-immunostained with human IgG (green) and different neuron markers ChAT (A, B) and PV (C, D). Images were taken under 20× object using an epifluorescence microscope with constant setting. 'Merge' images combine both channels to illustrate overlap. Scale bar: 40 μm. Uncropped images were used for automated quantification. Confocal images of higher magnification (40×) are shown in Figure S8A, Figure 3A, Figure S10A and Figure 3F.

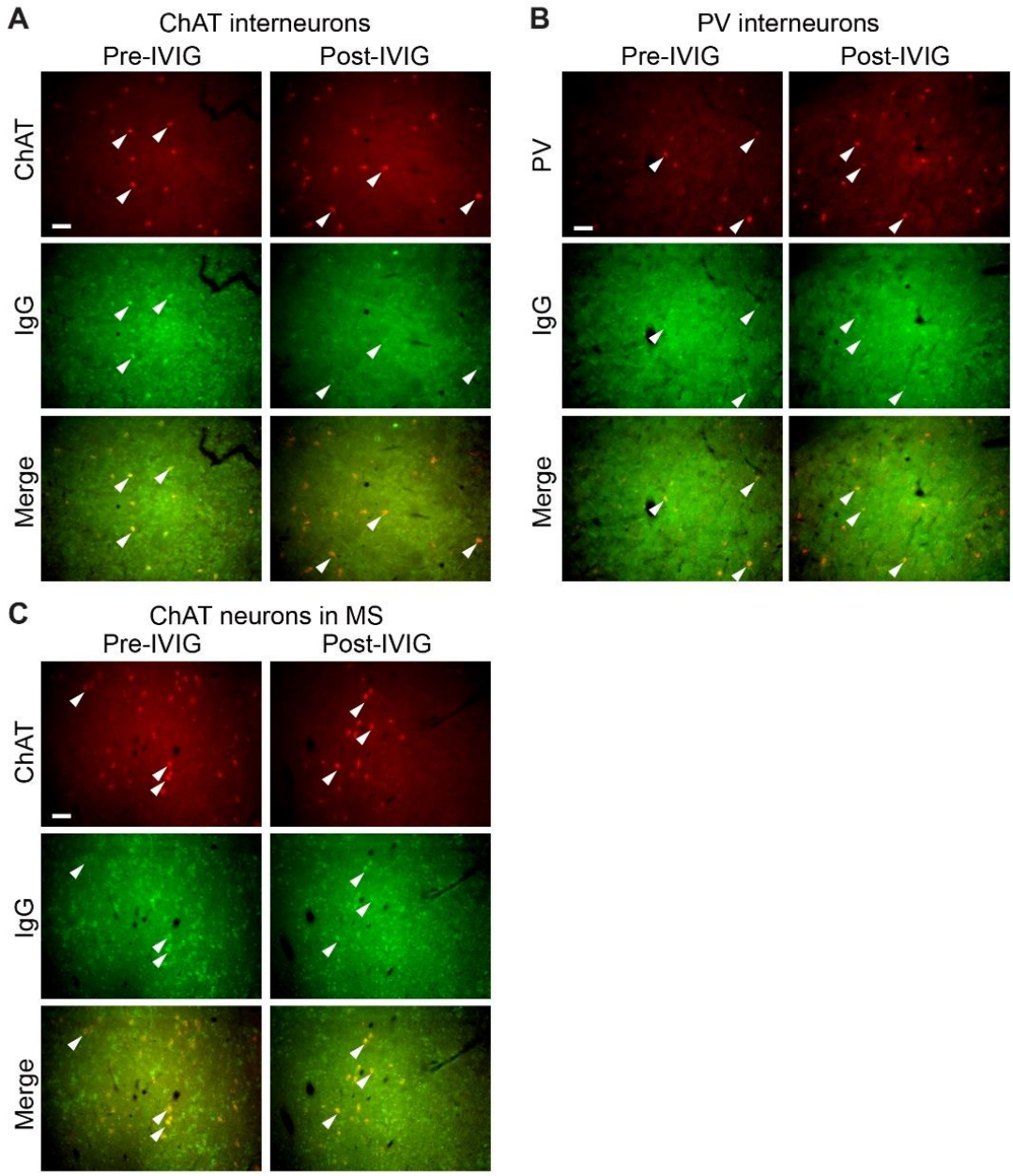

FIGURE S19. Representative images of serum IgG binding to several neuronal types following IVIG treatment. C57BL/6 mice striatal slices were treated with baseline (Pre-IVIG) and 3 months after intravenous immunoglobulin (IVIG) treatment (Post-IVIG) serum samples and co-immunostained with human IgG (green) and different neuron markers ChAT (A), PV (B) and ChAT in medial septum (C). Images were taken under 20× object using an epifluorescence microscope with constant setting. 'Merge' images combine both channels to illustrate overlap. Scale bar: 40 μm. Uncropped images were used for automated quantification. Confocal images of higher magnification (40×) are shown in Figure 4A and S14A,H.

TABLE S1. Subject demographics of the first and second cohorts

Subjects	Sex	Age (years)	Race/ Ethnicity[a]	Time of IVIG	Baseline CY-BOCS	Week 12 CY-BOCS	IgG titer (mg/dL) S1/S3
PANDAS							
1	F	9.5	M/NH	6	27	5	1250/1269
2	F	8.9	W/NH	0	28	0	898/1310
3	F	6.7	W/NH	0	27	11	1160/1200
4	M	8.2	W/NH	6	34	11	1120/1276
5	M	7.5	W/NH	0	27	9	1200/1379
6	F	7.7	W/NH	6	28	13	1310/1927
7	M	10.2	W/NH	0	24	0	745/776
8	M	12.1	W/NH	0	27	10	1170/884
9	M	4.2	W/NH	6	33	0	1100/1172
10	M	12.8	W	6	26	0	1150/1979
11	M	11.6	W/NH	6	34	3	1270/1089
Control							
1	F	8.0	W/NH	N/A	N/A	N/A	963/-
2	F	7.3	W/NH	N/A	N/A	N/A	1040/-
3	F	5.1	W/NH	N/A	N/A	N/A	896/-
4	M	7.8	M/H	N/A	N/A	N/A	877/-
5	M	8.1	M/NH	N/A	N/A	N/A	768/-
6	F	7.3	W/NH	N/A	N/A	N/A	1040/-
7	M	7.8	W/NH	N/A	N/A	N/A	877/-
8	M	10.6	W/NH	N/A	N/A	N/A	852/-
9	M	3.3	W/NH	N/A	N/A	N/A	513/-
10	M	11.5	W/NH	N/A	N/A	N/A	864/-
11	M	10.3	W/NH	N/A	N/A	N/A	888/-

[a] H: Hispanic; M: Multiple race; NH: non-Hispanic; W: White

TABLE S2. Subject demographics of the third cohort

Subjects	Sex	Age (years)	Race/Ethnicity	IgG titer (mg/dL)
PANDAS				
1	F	10.9	W/NH	663
2	M	8.1	W/H	526
3	F	11.9	W/NH	728
4	F	8.3	W/NH	802
5	M	6.0	W/NH	658
6	M	7.1	W/NH	777
7	M	9.8	W/NH	503
8	M	9.8	W/NH	922
9	M	8.3	W/NH	523
10	F	7.8	W/NH	1004
11	M	9.6	W/NH	953
12	F	10.7	W/NH	795
13	F	8.5	W/NH	832
14	M	6.8	W/NH	716
15	M	8.8	W/NH	651
16	M	7.5	W/NH	1147
Control				
1	F	8.9	W/NH	841
2	M	8.4	W/H	506
3	F	7.2	AA	916
4	M	6.2	M/H	1026
5	M	11.5	M/NH	902
6	M	10.7	W/NH	659
7	M	8.3	W/NH	813
8	F	7.6	W/NH	1021
9	M	10.3	W/NH	705
10	F	11.5	AA	973
11	F	4.9	W/NH	741
12	M	14.3	W/NH	1124

[a] AA: African American; H: Hispanic; M: Multiple race; NH: non-Hispanic; W: White

TABLE S3. Antibodies used in this study

Antibody	Immunogen	Host	Dilution	Source	Catalog#
anti-human IgG	IgG isolated from a pool of normal human sera	rabbit	1:200	Abcam, Cambridge, MA	ab2410
anti-ChAT	Human placental enzyme	goat	1:1000	Millipore, Billerica, MA	AB144P
anti-PV	Frog muscle parvalbumin	mouse	1:1000	Sigma, St. Louis, MO	P3088
anti-nNOS	Amino acids 2-300 of NOS1 of human origin	mouse	1:1000	Santa Cruz Biotechnology, Santa Cruz, CA	sc-5302
anti-FLAG	Synthetic peptide DYKDDDDK	mouse	1:1000	Sigma	F1804
anti-Myc	Synthetic peptide EQKLISEEDL	goat	1:1000	Abcam	ab9132
anti-phospho-rpS6 (Ser240/244)	Synthetic phosphopeptide corresponding to residues surrounding Ser240 and Ser244 of human ribosomal protein S6	rabbit	1:1000	Cell Signaling Danvers, MA	5364S
Alexa Fluor 488 donkey anti-rabbit	Heavy and light chains of Gamma immunoglobulins	donkey	1:800	Thermo Fisher Scientific, Fremont, CA	A21206
Alexa Fluor 594 donkey anti-goat	Heavy and light chains of Gamma immunoglobulins	donkey	1:800	Thermo Fisher Scientific	A11058
Alexa Fluor 594 donkey anti-mouse	Heavy and light chains of Gamma immunoglobulins	donkey	1:800	Thermo Fisher Scientific	A21203
HRP-conjugated goat anti-rabbit	Heavy and light chains of Gamma immunoglobulins	goat	1:10000	Thermo Fisher Scientific	31430

TABLE S4. Intrinsic membrane properties of striatal cholinergic interneurons after serum pretreatment

	RMP (mV)	Spike Threshold (mV)	Spike Width (ms)	AHP amplitude (mV)
Control	65.7 ± 1.5 (n = 15)	52.4 ± 1.3 (n = 15)	4.3 ± 0.4 (n = 15)	12.2 ± 0.78 (n = 15)
PANDAS	66.4 ± 1.8 (n = 14)	51.2 ± 1.4 (n = 14)	4.6 ± 0.7 (n = 14)	9.7 ± 1.1 (n = 14)

REFERENCES

1. Williams KA, Swedo SE, Farmer CA, Grantz H, Grant PJ, D'Souza P, Hommer R, Katsovich L, King RA, Leckman JF. Randomized, Controlled Trial of Intravenous Immunoglobulin for Pediatric Autoimmune Neuropsychiatric Disorders Associated With Streptococcal Infections. J Am Acad Child Adolesc Psychiatry. 2016;55:860-867.
2. Frick LR, Rapanelli M, Jindachomthong K, Grant P, Leckman JF, Swedo S, Williams K, Pittenger C. Differential binding of antibodies in PANDAS patients to cholinergic interneurons in the striatum. Brain Behav Immun. 2018;69:304-311.
3. Bateup HS, Svenningsson P, Kuroiwa M, Gong S, Nishi A, Heintz N, Greengard P. Cell type-specific regulation of DARPP-32 phosphorylation by psychostimulant and antipsychotic drugs. Nat Neurosci. 2008;11:932-939.
4. Rapanelli M, Frick L, Jindachomthong K, Xu J, Ohtsu H, Nairn AC, Pittenger C. Striatal Signaling Regulated by the H3R Histamine Receptor in a Mouse Model of tic Pathophysiology. Neuroscience. 2018;392:172-179.
5. Bertran-Gonzalez J, Chieng BC, Laurent V, Valjent E, Balleine BW. Striatal cholinergic interneurons display activity-related phosphorylation of ribosomal protein S6. PLoS One. 2012;7:e53195.